Journal of The Electrochemical Society

The Electrochemical Society
Advancing solid state & electrochemical science & technology

OPEN ACCESS

Diphenyl Diselenide as SEI-forming Additive for a High-voltage $LiCoO_2$/Graphite Battery

To cite this article: Hyeonghun Park and Hyeong-Jin Kim 2020 *J. Electrochem. Soc.* **167** 070555

Journal of The Electrochemical Society, 2020 **167** 070555

Diphenyl Diselenide as SEI-forming Additive for a High-voltage $LiCoO_2$/Graphite Battery

Hyeonghun Park and Hyeong-Jin Kim[*,z]

Graduate Program of Energy Technology, School of Integrated Technology, Gwangju Institute of Science and Technology, Gwangju 61005, Republic of Korea

In this study, we investigate the effect of diphenyl diselenide (DPDS) as a bifunctional additive on $LiCoO_2$/graphite batteries charged to 4.4 V. In the 3.0–4.4 V potential window, a $LiCoO_2$/graphite full cell suffers from poor cycle performance, with a capacity retention of 88.7% after 200 cycles. With the addition of 0.1 wt% DPDS, the capacity retention is increased to 95.2% after 200 cycles. Linear sweep voltammetry (LSV) and cyclic voltammetry (CV) experiments indicate that DPDS is oxidized and reduced prior to the decomposition of the electrolyte. Density functional theory (DFT) calculations theoretically show that DPDS has higher highest occupied molecular orbital (HOMO) and lower lowest unoccupied molecular orbital (LUMO) energy levels than the electrolyte. Field-emission scanning electron microscopy (FE-SEM), electrochemical impedance spectroscopy (EIS), X-ray photoelectron spectroscopy (XPS) and X-ray diffraction (XRD) analyses demonstrate that DPDS is decomposed at the $LiCoO_2$ and graphite surface and modifies the properties of the SEI layer. As a result, the improved battery performance enabled by diphenyl diselenide can be attributed to the SEI layers preventing collapse of the $LiCoO_2$ crystal on the cathode and decreasing the reactions of graphite with the electrolyte on the anode.

 [DOI: 10.1149/1945-7111/ab80cf]

Manuscript submitted December 28, 2019; revised manuscript received March 9, 2020. Published April 8, 2020. *This paper is part of the JES Focus Issue on Challenges in Novel Electrolytes, Organic Materials, and Innovative Chemistries for Batteries in Honor of Michel Armand.*

Over the past two decades, lithium-ion batteries (LIBs) have been improved significantly. However, as the use of electronic devices and electric vehicles increases, there is still a demand for higher energy density and power density.[1–3] To satisfy this demand, several studies have been conducted. For example, Ni-rich cathode materials such as NMC 622 and NMC 811 were synthesized,[4] 3D-structured current collectors[5] were used, and laser structuring was applied to the electrode.[6] However, the easiest way to achieve higher energy is to raise the charging voltage of batteries. $LiCoO_2$, the flagship cathode material of LIBs, is typically charged to 4.2 V, but a higher capacity can be obtained by charging above 4.2 V. However, charging above 4.2 V causes oxidation of the electrolyte at the cathode surface, which generates a thick solid-electrolyte interface (SEI) layer on the $LiCoO_2$ cathode and leads to capacity degradation during cycling.[7,8]

To improve its high voltage performance, surface treatment of $LiCoO_2$ with metal oxides such as Al_2O_3, $AlPO_4$, TiO_2, and CoO has been used.[9–12] However, this metal oxide coating process has difficulty in controlling the coating composition, and there is a limit to the improvement in electrochemical characteristics using the coating method while maintaining the properties of $LiCoO_2$ due to the low ionic and electric conductivities of the metal oxide.[13,14] Moreover, this coating methods necessitates complex and expensive processes. To counter these limitations, studies on finding an easy and effective coating method by adding electrolyte additives have been conducted.

The SEI layer formed on the anode is well known, and electrolyte additives for anodes such as fluoroethylene carbonate and succinic anhydride are also well established.[15,16] However, electrolyte additives that are effective for both the anode and cathode (bifunctional additive) are ideal because the SEI layer is also formed on the cathode.[17–19] Eom et al. reported that a Se-derived SEI layer at the anode surface has high ionic conductivity and solvent penetration resistivity.[20] To use Se as a bifunctional additive, preferential oxidation of Se over ethylene carbonate (EC) and diethyl carbonate (DEC) is required.

Diphenyl diselenide (DPDS; its structure is shown in Fig. 1), an organo-selenium compound, has a phenyl group, which is an electron-donating group. This electron-donating group increases the energy level of the highest occupied molecular orbital (HOMO), and consequently, DPDS is oxidized before electrolyte decomposition.[21] Herein, DPDS is investigated as a bifunctional additive to improve battery performance in high-voltage $LiCoO_2$/graphite batteries. Electrochemical analysis demonstrates that DPDS has a positive effect on the cycle performance of the $LiCoO_2$/graphite battery.

Experimental

Preparation of electrodes and electrolyte.—The $LiCoO_2$ slurry was composed of 92 wt% $LiCoO_2$ (L&F, Korea), 4 wt% conductive carbon and 4 wt% polyvinylidene fluoride (PVDF) with N-methyl pyrrolidone. The graphite slurry was composed of 96 wt% graphite (Hitachi, Japan), 1 wt% super-P, 1.5 wt% carboxymethyl cellulose (CMC) and 1.5 wt% styrene butadiene rubber (SBR) in H_2O. The $LiCoO_2$ slurry was coated onto Al foil with a loading density of 18.49 mg cm^{-2}. The graphite slurry was coated onto Cu foil with a loading density of 8.11 mg cm^{-2}. Ethylene carbonate (EC), diethyl carbonate (DEC) and lithium hexafluorophosphate ($LiPF_6$) were used in the experiment as the solvents and lithium salt, respectively, and these materials were obtained from SoulBrain Co., Ltd. Electrolytes were prepared by stirring EC/DEC (1:1 v/v) with 1 M $LiPF_6$ and diphenyl diselenide (DPDS, Sigma Aldrich) as an additive in an argon-filled glove box (Mbodytech, Korea, H_2O < 1 ppm).

All 2032-type coin cells (NEBA, Korea) were assembled in an argon-filled glove box. All electrodes were dried in a vacuum oven for 24 h at 70 °C before assembly. A polypropylene separator (Celgard 2400, USA) and a 1.3 mm stainless steel spacer were used. A total of 50 μl of electrolyte with/without DPDS was added to the cell. The coin cells used for cyclic voltammetry were assembled using a lithium metal chip (NEBA, Korea) as the anode and $LiCoO_2$ and graphite as the cathodes.

Measurement.—The LSV measurement was conducted on electrochemical equipment (VSP, Biologic, France) using a three-electrode cell with a 16 mm platinum disk as the working electrode,

*Electrochemical Society Member.
[z]E-mail: hjkimc@gist.ac.kr

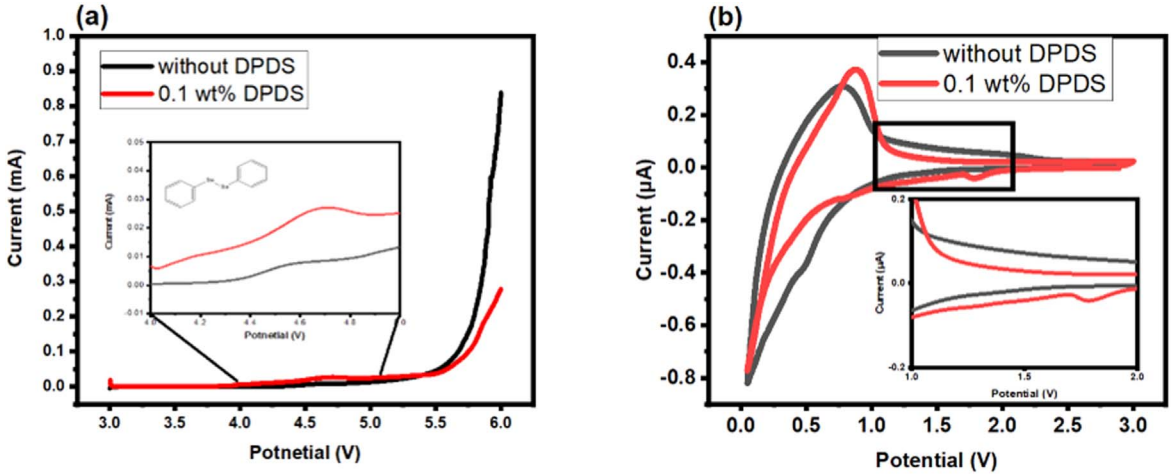

Figure 1. linear sweep voltammograms (a) of platinum electrodes; (b) cyclic voltammograms of graphite/Li in the electrolyte with and without DPDS at a scan rate of (a) 0.1 mV s^{-1}; (b) 1.0 mV s^{-1}.

a lithium metal chip as the counter electrode and a lithium-coated stainless steel ring as the reference electrode at a scan rate of 0.1 mV s^{-1}. The CV measurement was also conducted on a Biologic-VSP potentiostat in Li/graphite half cells at a scan rate of 1.0 mV s^{-1}. EIS measurements were conducted on fully discharged cells after 5 cycles and 200 cycles using the Biologic-VSP potentiostat, and the impedance frequency ranged from 100 kHz to 0.01 Hz with an amplitude of 10 mV.

All galvanostatic measurements were conducted using a battery cycler (WBCS 3000, Wonatech, Korea). The charging process of the $LiCoO_2$/graphite cells was carried out with a constant current (1 C rate) until the cells were charged to 4.4 V, and then the cells were charged with a constant voltage of 4.4 V until the current decreased to one-tenth of the charge current. In the case of discharging, the cells were discharged to 3.0 V with a constant current (1 C rate). All cells underwent 5 SEI formation cycles with CC–CV charging with 0.1 C and CC discharging with 0.1 C. The charge/discharge current was 1 C rate for the cycling test, whereas various rates ranging from 0.1 C rate to 3 C rate were used for the rate capability test. All electrochemical measurements were conducted at 25 °C.

After cycling, the cells were disassembled in an argon-filled glove box for material characterization. The electrodes were rinsed with dimethyl carbonate (Sigma Aldrich) to eliminate the stained electrolyte, salt, and additive. The samples were dried in an argon-filled glove box for 12 h. After drying, the electrodes were stored in a vacuum oven to prevent contact with oxygen. FE-SEM (Gemini 500, ZEISS, Germany) was used to observe electrode surface morphology. The crystal structure of the cycled $LiCoO_2$ cathode and graphite anode was observed by X-ray diffraction with Cu Kα radiation (Bruker, D8 Advance, Germany). An X-ray photoelectron spectrometer (ESCALAB 250Xi, Thermo Scientific, USA) was used to analyze the electrode surface.

Results and Discussion

Design and SEI-forming tendency of DPDS as a bifunctional additive.—The oxidation and reduction reactions of DPDS were measured using LSV and CV to understand the SEI-forming ability of DPDS on the $LiCoO_2$ cathode and graphite anode in electrolyte of EC:DEC (1:1 v/v) with 1 M $LiPF_6$. As shown in Fig. 1a, presenting the linear sweep voltammograms of the standard electrolyte and electrolyte with 0.1 wt% DPDS with a platinum working electrode, the standard electrolyte was decomposed at 5.0 V, where the current peak was observed. On the other hand, the electrolyte with 0.1 wt% DPDS started to decompose from 3.7 V and peak was observed at 4.6 V. It is known that HOMO and LUMO energy levels are related to the ability to gain and lose electrons.[22] The G09 B3LYP/6–311++G(d, p) basis set was used to calculate the HOMO and LUMO energy levels of EC and DEC, and the results are shown in Table I. As indicated by these results, DPDS has a higher HOMO energy level (−6.25 eV) than EC (−8.47 eV) and DEC (−8.06 eV), which indicates that DPDS was oxidized before EC and DEC on the cathode. As a result, DPDS-derived SEI layer was formed and suppressed repeated electrolyte decomposition. As shown in Fig. 1b,

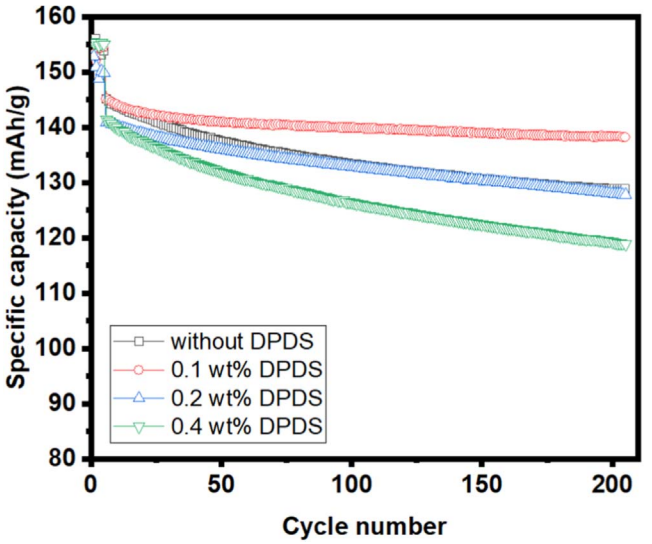

Figure 2. Cycle performance of $LiCoO_2$/graphite full cells at 25 °C.

Table I. HOMO and LUMO energy levels of EC, DEC and DPDS.

Electrolyte and additive	HOMO (eV)	LUMO (eV)	Oxidation potential (eV)
EC	−8.47	−0.60	8.73
DEC	−8.06	−0.27	8.28
DPDS	−6.25	−2.13	5.71

a reduction peak at 1.8 V can be observed for the electrolyte with 0.1% DPDS, in contrast to the standard electrolyte. This peak is attributed to the reduction current of DPDS before EC and DEC. Furthermore, the reduction peak at 0.1 V remarkably decreases. As indicated in Table I, the LUMO energy level of DPDS (−2.13 eV) is lower than that of EC (−0.60 eV) and DEC (−0.27 eV), which indicates that DPDS can also be reduced before EC and DEC on the anode, suggesting that DPDS participates in the SEI layer formation process on graphite and suppresses the anode-electrolyte reaction.

Charge/discharge test and rate performance.—To monitor the effects of DPDS on the cyclic stabilities of $LiCoO_2$/graphite cells at a high cut-off voltage, $LiCoO_2$/graphite cells with and without DPDS were tested at 1 C rate. As shown in Fig. 2, the cell without DPDS shows poor cycle performance with only 88.7% capacity retention, as well as capacity degradation from 145.1 mAh g^{-1} to 128.8 mAh g^{-1} after 200 cycles within a potential window of 3.0–4.4 V. As shown in Fig. 2, the cell with 0.1% DPDS shows the best cycle performance, exhibiting 95.2% capacity retention with capacity degradation from 145.1 mAh g^{-1} to 138.1 mAh g^{-1} after 200 cycles within a potential window of 3.0–4.4 V. This improved result can be explained by DPDS-induced SEI layer formation at the electrode surface because this SEI layer effectively suppresses successive electrolyte decomposition. In contrast, only 78.3% capacity retention with capacity degradation from 141.4 mAh g^{-1} to 118.9 mAh g^{-1} after 200 cycles is obtained from the cell with 0.4 wt% DPDS.

These results are related to the thick SEI layer formed on the electrode surface. Due to concentrations of DPDS higher than 0.1 wt %, a thick SEI layer containing DPDS is formed on $LiCoO_2$ and graphite. The thick SEI layer blocks lithium-ion migration and increases resistance, resulting in capacity decay. The ratio of charge and discharge capacity, or initial Coulombic efficiency (ICE), is related to the consumption of lithium ion used to produce solid electrolyte interface (SEI) layer. As shown in Table II, ICE decreases with increasing DPDS concentration. In other word, high concentration of DPDS makes more SEI layer.[23]

The rate capabilities of $LiCoO_2$/graphite cells with/without DPDS at 3.0–4.4 V are presented in Fig. 3. As shown in Fig. 3, the cells with 0.2 wt% and 0.4 wt% DPDS showed a lower capacity than the other cells, especially in the 0.4 wt% cell. The capacity difference increases as the current increases. This result indicates that the electrolyte with 0.4 wt% DPDS formed a thick SEI layer on the $LiCoO_2$ and graphite surface. The thick SEI layer that is formed due to decomposition of the excess additive disrupts Li^+ ion diffusion during lithiation/delithiation, inducing a decrease in capacity. In contrast, the cell with 0.1 wt% DPDS is barely different from the cell without DPDS; rather, it exhibits a slightly high capacity at 3 C. This result indicates that the SEI layer decomposed from the electrolyte containing 0.1 wt% DPDS does not disrupt Li^+ ion diffusion during lithiation and delithiation.

Electrochemical impedance spectroscopy analysis.—To identify the effect of DPDS on the $LiCoO_2$ and graphite surface, electrochemical impedance spectroscopy (EIS) test was performed. Commonly, high-frequency semicircles indicate solid electrolyte interface resistance (R_{SEI}), and middle-frequency semicircles indicate charge transfer resistance (R_{ct}) for Li^+ ions at the surface.[24,25] As shown in Fig. 4, the cell with 0.1 wt% DPDS shows a lower

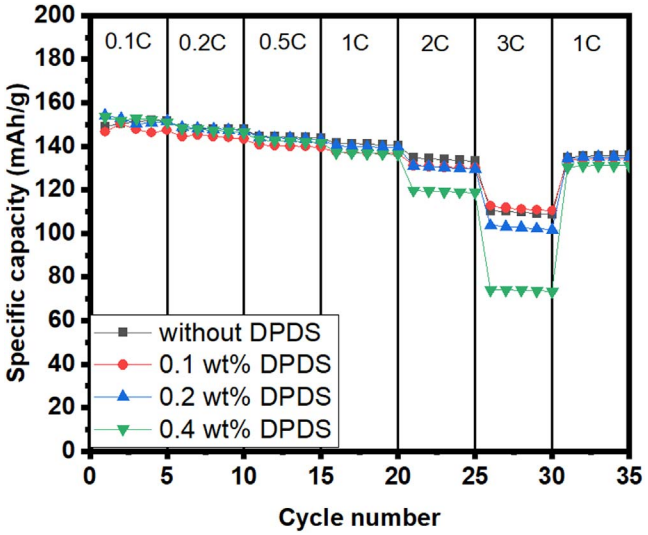

Figure 3. Rate performance of the $LiCoO_2$/graphite full cell at 25 °C.

semicircle after 200 cycles (100% discharged) at middle-frequency, which indicates the formation of a positive SEI layer during the charging process to 4.4 V. This result proves that the SEI layer, including DPDS, is effective for lithiation and delithiation and functions as a protective barrier from further reactions between the electrode and electrolyte, thereby reducing the cell impedance. The interesting point is the small impedance circle of the cell with 0.2 wt % DPDS. The cell with 0.2 wt% DPDS exhibited lower performance in the discharge capacity and rate capability test than the cell without DPDS, despite having small impedance circles. This result might be due to the concentration near 0.2 wt% being the threshold for using DPDS.

Field-emission scanning electron microscopy morphology of the electrodes.—The field-emission scanning electron microscopy (FE-SEM) morphologies of the $LiCoO_2$ cathode and graphite anode with/without DPDS are presented in Fig. 5. As shown in Fig. $5a_1$, the fresh $LiCoO_2$ particles have a smooth surface. As shown in Fig. $5a_2$, in the case of charging up to 4.4 V, cracks are observed on the surface of $LiCoO_2$ after 200 cycles, indicating that the protective SEI layer is not formed on the $LiCoO_2$ surface. The $LiCoO_2$ particles charged up to 4.4 V without DPDS were damaged (Fig. $5a_2$) due to the phase transition between the hexagonal and monoclinic phases.[19] In contrast, the cycled $LiCoO_2$ with 0.1% DPDS retains its initial morphology, as shown in Fig. $5a_3$. These results indicate that DPDS participates in SEI layer formation on the $LiCoO_2$ cathode and prevents unwanted cathode-electrolyte reactions.[26–28] As shown in Fig. $5b_1$, the fresh graphite particles have a smooth surface. As shown in Fig. $5b_2$, in the case of charging up to 4.4 V, the SEI layer of the decomposed electrolyte is observed on the surface of graphite after 200 cycles. This thick SEI layer prevents lithiation and delithiation and induces capacity degradation.[27] On the other hand, a dense SEI layer is observed on the graphite surface after 200 cycles, as shown in Fig. $5b_3$. This SEI layer protects the graphite anode from direct electrolyte-electrode reactions. As a result, the

Table II. Initial Coulombic efficiency of $LiCoO_2$/graphite full cells at 25 °C.

Concentration	Discharge capacity (mAh g^{-1})	Charge capacity (mAh g^{-1})	ICE
0%	155.189	181.768	0.854
0.1%	153.262	187.815	0.816
0.2%	152.959	199.243	0.768
0.4%	155.375	207.293	0.750

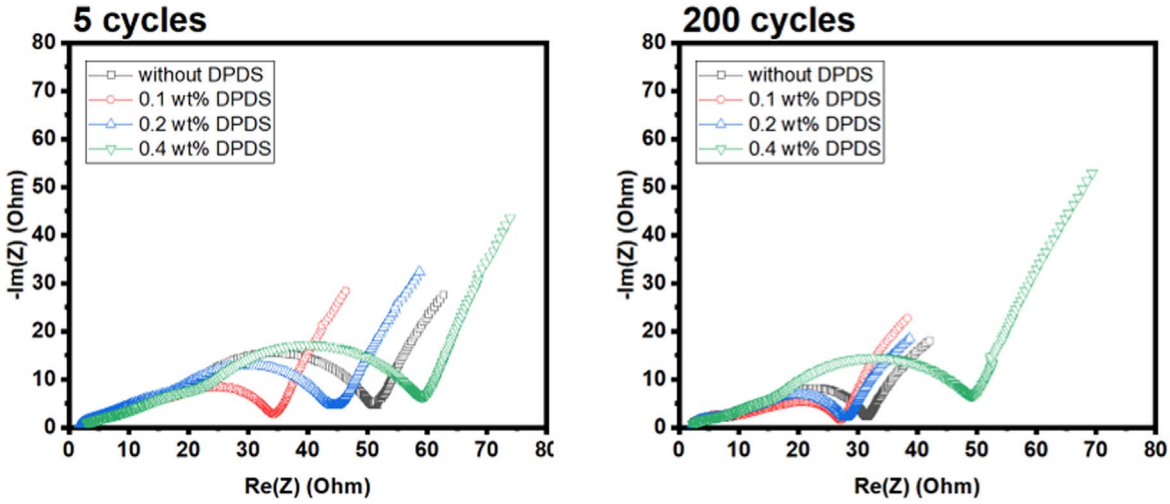

Figure 4. Electrochemical impedance spectra of $LiCoO_2$/graphite full cells with different amounts of DPDS charged to 4.4 V.

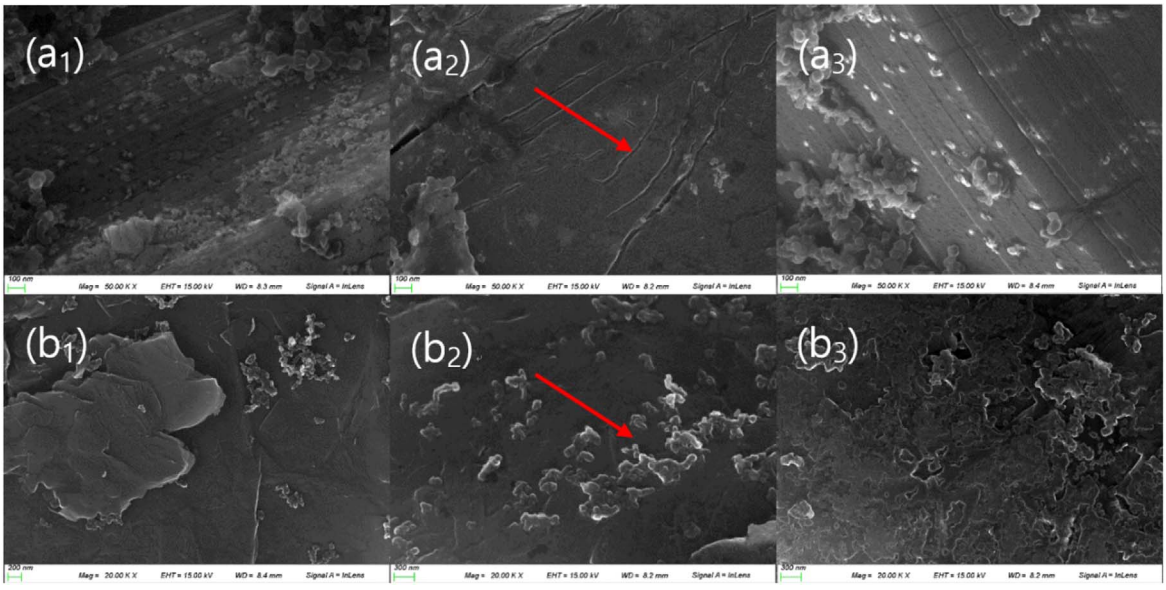

Figure 5. FE-SEM morphologies of the (a) $LiCoO_2$ cathodes and (b) graphite anodes: fresh electrodes (a_1, b_1) and electrodes after 200 cycles without DPDS (a_2, b_2) and with 0.1 wt% DPDS (a_3, b_3).

irreversible capacity loss and capacity degradation of the cell are decreased.

X-ray photoelectron spectroscopy.—To further investigate the effect of DPDS on the electrode surfaces, X-ray photoelectron spectroscopy (XPS) was conducted. It is well known that initial SEI formation has a significant effect on SEI composition.[29] Therefore, XPS was conducted after 5 SEI formation cycles. XPS spectra of $LiCoO_2$ are provided in Fig. 6. The cathode spectra were calibrated by the C–C peak at a binding energy of 284.3 eV. The C1s spectrum of the $LiCoO_2$ electrode includes five peaks. The C–C (284.3 eV) peak is assigned to acetylene black, and the C–H (285.5 eV) and C–F (290.3 eV) peaks correspond to the PVDF binder.[26,30,31] Two peaks, C–O (286.5 eV) and C=O (288.0 eV), are related to $ROCO_2Li$ and ROLi, which can be formed by electrolyte decomposition.[26] Higher C–C, C–H and C–F peaks are observed from the cell with the electrolyte containing 0.1 wt% DPDS than the cell with the electrolyte without DPDS. However, a low C=O peak and no C–O peak are detected with 0.1 wt% DPDS, indicating that a thin SEI layer is formed and consequently does not interfere with the detection of acetylene black and PVDF. The O1s spectrum includes three peaks: M–O (529.2 eV), which is related to the metal oxide bonds in the cathode material; C=O (532.0 eV); and C–O (533.5 eV).[31,32] The M–O peak with 0.1 wt% DPDS is higher than the peak with the standard electrolyte, suggesting that a thin SEI layer is formed. For the same reason, the C=O and C–O peaks are dramatically decreased. LiF (685.0 eV), $Li_xPO_yF_z$ (686.2 eV) peaks, which are originated from decomposition of $LiPF_6$, and C–F (687.6 eV, PVDF) peak are observed in the F1s spectrum.[31,33] The LiF peaks in the two spectra show the same intensity, and C–F shows a slightly higher intensity in $LiCoO_2$ with 0.1 wt% DPDS than in $LiCoO_2$ without DPDS. However, compared to the case without DPDS where Li_xPOyF_z was strongly observed, the peak of $Li_xPO_yF_z$ is hardly observed with DPDS. This result means that electrolyte decomposition is effectively suppressed by DPDS. The P2p spectrum presents $Li_xPO_yF_z$ (135.0 eV) and Li_xPF_y (136.7 eV) peaks.[31,33] The lower intensity of both peaks confirms that decomposition products of DPDS form protective films. The peak at 141.6 eV has not been reported in an SEI layer derived from $LiPF_6$. Since this work is the first paper that reported this peak, more research on the reaction of DPDS and $LiPF_6$ is needed.

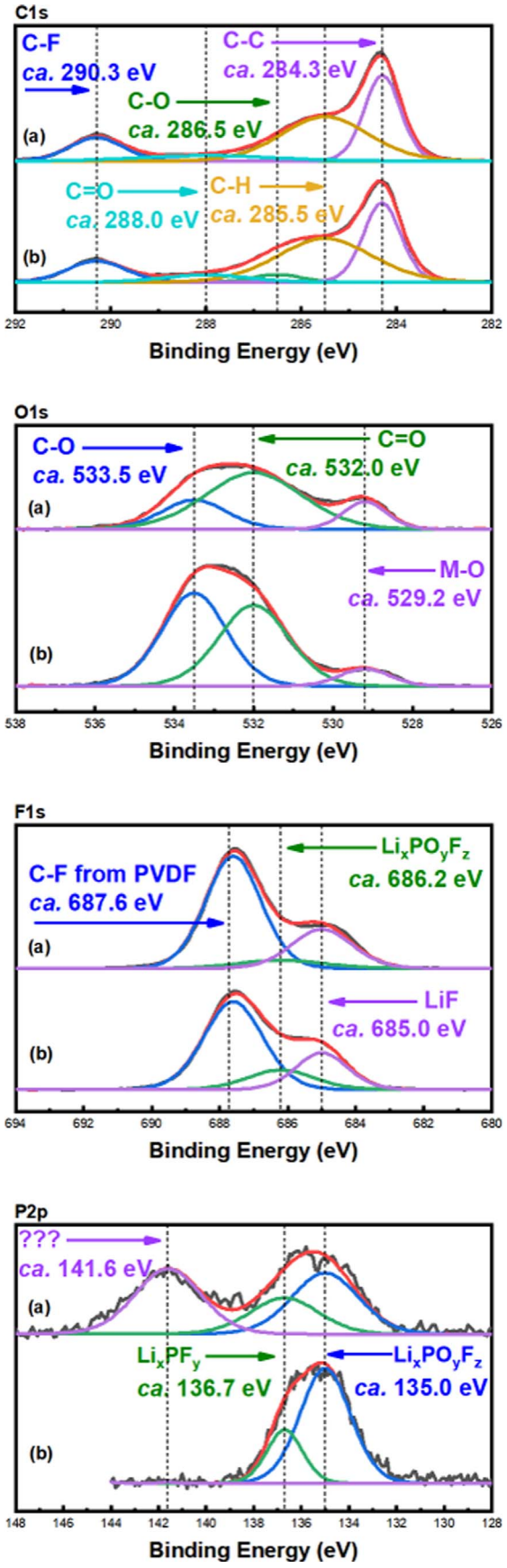

Figure 6. C1s, O1s, F1s, and P2p XPS spectra of the $LiCoO_2$ cathode after 5 cycles (a) with and (b) without DPDS.

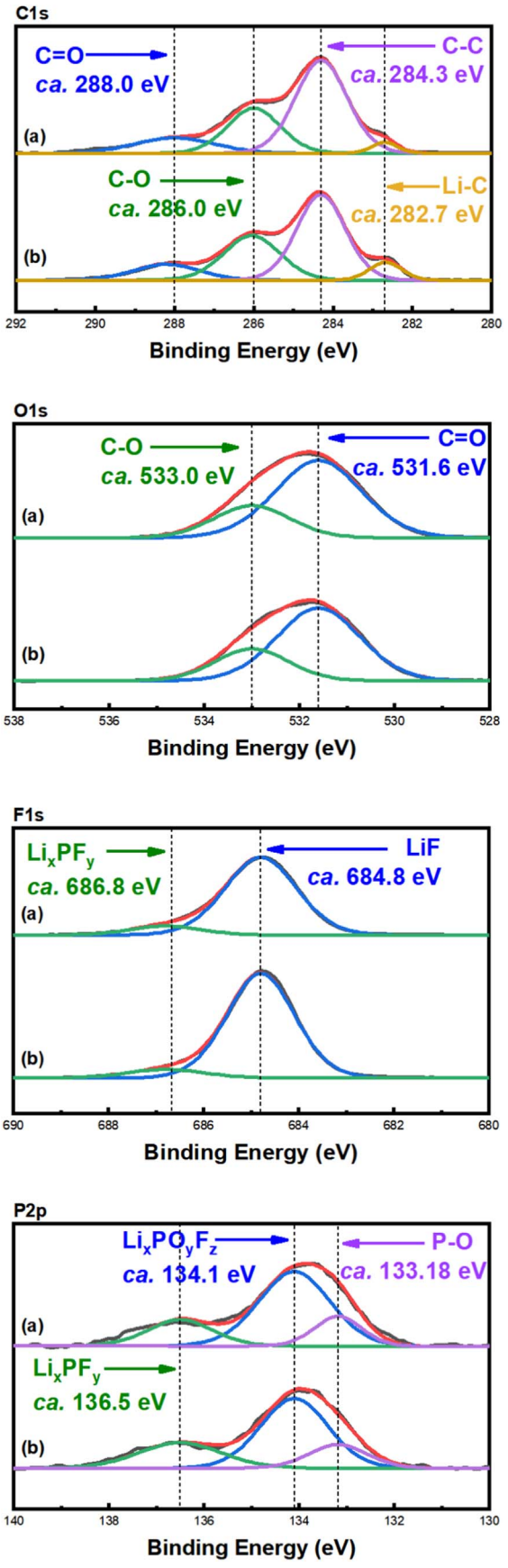

Figure 7. C1s, O1s, F1s, and P2p XPS spectra of the graphite anode after 5 cycles (a) with and (b) without DPDS.

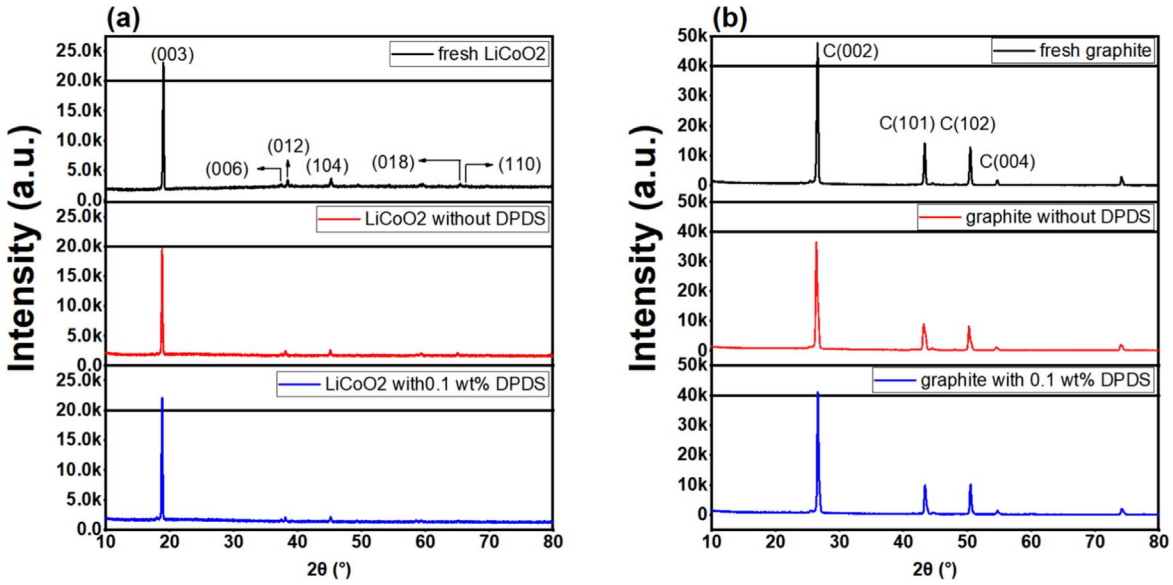

Figure 8. XRD patterns of the (a) $LiCoO_2$ cathode and (b) graphite anode with/without DPDS after 200 cycles.

The XPS spectra of graphite are also shown in Fig. 7. The anode spectra are also calibrated by the C–C peak at a binding energy of 284.3 eV. The C1s spectrum of the graphite electrode includes four peaks. The Li–C (282.7 eV) peak corresponds to electrolyte decomposition species such as carbonate and lithium carbide, and the C–C (284.3 eV) peak is assigned to graphite or a conductive agent.[33,34] The C–O (286.0 eV) and C=O (288.0 eV) peaks correspond to lithium alkyl carbonate.[35] A lower Li-C peak is detected at the graphite anode with 0.1 wt% DPDS than the graphite anode without DPDS, suggesting less electrolyte reduction. Two peaks, LiF (684.8 eV) and Li_xPF_y (686.8 eV), are observed in the F1s spectrum.[33,36] The F1s spectrum of the graphite anode without DPDS has a higher peak at 684.8 eV than that of the corresponding spectrum of the graphite anode with 0.1 wt% DPDS, consistent with the higher electrolyte decomposition in the former case. The C=O (531.6 eV) and C–O (533.0 eV) peaks in the O1s spectrum are assigned to lithium alkyl carbonate.[35,36] In the P2p spectra, three peaks, P–O (133.18 eV), $Li_xPO_yF_z$ (134.1 eV) and Li_xPF_y (136.5 eV), are detected.[37] There are no particular differences in the O1s and P2p spectra. It may be because XPS was implemented after 5 initial SEI formation cycle. In the initial SEI, inorganic component such as LiF is mainly formed.[38] After repetitive SEI formation reaction, $Li_xPO_yF_z$ or organic components are formed in SEI.[39] As a result, no significant difference was observed in the spectra except Li-C and LiF. More clear difference will be confirmed using long cycle electrodes.

X-ray diffraction.—Crystal analysis is performed on the $LiCoO_2$ cathode and graphite anode after 200 cycles to analyze the crystal phase. The obtained XRD patterns of the $LiCoO_2$ cathode are presented in Fig. 8a. Clear layered structure peaks, (006)/(012) and (018)/(110), are observed in the pattern of the fresh $LiCoO_2$ cathode.[9,27] However, the intensities of the (003) and (006) peaks sharply decrease after 200 cycles in the cathode without DPDS. This result indicates that an ineffective SEI layer was formed on the $LiCoO_2$ surface without DPDS; consequently, the layered structure is not protected. In contrast, as shown in Fig. 8a, the peaks of the cathode with 0.1% DPDS are maintained. This result indicates that an effective SEI layer was formed on the $LiCoO_2$ surface; consequently, the crystal structure can be maintained. As shown in Fig. 8b, presenting the XRD patterns of the graphite anode, the graphite structure with (002) and (004) orientations can be observed.[27] For the electrode without DPDS, these graphite peaks decrease after 200 cycles, indicating that the layered graphite structure is destroyed. However, the pristine peaks of the layered structure are well maintained in the cell containing 0.1 wt% DPDS, suggesting that the DPDS-derived SEI layer acted as a passivation layer and consequently can protect the layered graphite structure.

Conclusions

In this study, we seek to improve the performance of a $LiCoO_2$/graphite battery in a high-voltage window (3.0–4.4 V) using DPDS as a bifunctional additive. First, it was demonstrated that the SEI layer formed due to prior decomposition of DPDS, which can protect the $LiCoO_2$ and graphite surface from successive electrolyte reactions and structural destruction. LSV, CV, DFT, FE-SEM, XRD, and XPS analyses reveal that the DPDS-derived SEI layer can protect $LiCoO_2$ and graphite due to the preferential decomposition of DPDS. A suitable concentration of DPDS forms a stable SEI layer, which yields a positive effect. Consequently, DPDS significantly enhances the cycling performance of a high-voltage $LiCoO_2$/graphite battery.

Acknowledgments

This work was supported by GIST Research Institute (GRI) grant funded by Gwangju Institute of Science Technology in 2020.

ORCID

Hyeonghun Park https://orcid.org/0000-0001-9579-5245
Hyeong-Jin Kim https://orcid.org/0000-0003-1663-7690

References

1. J. B. Goodenough and K.-S. Park, *JACS*, **135**, 1167 (2013).
2. M. Hu, X. Pang, and Z. Zhou, *J. Power Sources*, **237**, 229 (2013).
3. B. Li, L. Xing, M. Xu, H. Lin, and W. Li, *Electrochem. Commun.*, **34**, 48 (2013).
4. R. Jung, M. Metzger, F. Maglia, C. Stinner, and H. A. Gasteiger, *J. Electrochem. Soc.*, **164**, 1361 (2017).
5. C. Yang, Y. Yin, S. Zhang, N. Li, and Y. Guo, *Nat. Commun.*, **6**, 8058 (2015).
6. P. Smyrek, J. Pröll, H. J. Seifert, and W. Pfleging, *J. Electrochem. Soc.*, **163**, 19 (2015).
7. S.-Y. Ha, J.-G. Han, Y.-M. Song, M.-J. Chun, S.-I. Han, W.-C. Shin, and N.-S. Choi, *Electrochim. Acta*, **104**, 170 (2013).
8. R. Yazami, Y. Ozawa, H. Gabrisch, and B. Fultz, *Electrochim. Acta*, **50**, 385 (2004).
9. L. Liu, Z. Wang, H. Li, L. Chen, and X. Huang, *Solid State Ionics*, **152–153**, 341 (2002).
10. B. Kim, J.-G. Lee, M. Choi, J. Cho, and B. Park, *J. Power Sources*, **126**, 190 (2004).
11. A. Zhou, Y. Lu, Q. Wang, J. Xu, W. Wang, X. Dai, and J. Li, *J. Power Sources*, **346**, 24 (2017).
12. S. Jeong, J. Kim, and J. Mun, *J. Electrochem. Soc.*, **166**, A5038 (2019).

13. J. Xie, J. Zhao, Y. Liu, H. Wang, C. Liu, T. Wu, P.-C. Hsu, D. Lin, Y. Jin, and Y. Cui, *Nano Res.*, **10**, 3754 (2017).
14. Y. S. Jung, A. S. Cavanagh, A. C. Dillon, M. D. Groner, S. M. George, and S.–H. Lee, *J. Electrochem. Soc.*, **157**, A75 (2010).
15. X.–Q. Zhang, X.–B. Cheng, X. Chen, C. Yan, and Q. Zhang, *Adv. Funct. Mater.*, **27**, 1605989 (2017).
16. H. Lee, S. Choi, S. Choi, H.–J. Kim, Y. Choi, S. Yoon, and J.–J. Cho, *Electrochem. Commun.*, **9**, 801 (2007).
17. K. Abe, Y. Ushigoe, H. Yoshitake, and M. Yoshio, *J. Power Sources*, **153**, 328 (2006).
18. K. Abe, T. Takaya, H. Yoshitake, Y. Ushigoe, M. Yoshio, and H. Wang, *Electrochem. Solid-State Lett.*, **7**, 462 (2004).
19. J. Cho, Y. J. Kim, T.-J. Kim, and B. Park, *Angew. Chem. Int. Ed.*, **40**, 3367 (2001).
20. K. Eom, J. T. Lee, M. Oschatz, F. Wu, S. Kaskel, G. Yushin, and T. F. Fuller, *Nat. Commun.*, **8**, 13888 (2017).
21. T. Sutradhar and A. Misra, *The Journal of Physical Chemistry A*, **122**, 4111 (2018).
22. Z. Zhang, L. Hu, H. Wu, W. Weng, M. Koh, P. C. Redfern, L. A. Curtiss, and K. Amine, *Energy Environ. Sci.*, **6**, 1806 (2013).
23. F. Zhang, G. Zhu, K. Wang, X. Qian, Y. Zhao, W. Luo, and J. Yang, *Journal of Materials Chemistry A*, **7**, 17426 (2019).
24. M. D. Levi, G. Salitra, B. Markovsky, H. Teller, D. Aurbach, U. Heider, and L. Heider, *J. Electrochem. Soc.*, **146**, 1279 (1999).
25. C. Wang, X. Zuo, M. Zhao, X. Xiao, L. Yu, and J. Nan, *J. Power Sources*, **307**, 772 (2016).
26. S. Mai, M. Xu, X. Liaom, L. Xing, and W. Li, *J. Power Sources*, **273**, 816 (2015).
27. M. Zhao, X. Zuo, X. Ma, X. Xiao, L. Yu, and J. Nan, *J. Power Sources*, **323**, 29 (2016).
28. X. Zuo, M. Zhao, X. Ma, X. Xiao, J. Liu, and J. Nan, *Electrochim. Acta*, **245**, 705 (2017).
29. A. Wang, S. Kadam, H. Li, S. Shi, and Y. Qi, *NPJ Comput. Mater.*, **4**, 1 (2018).
30. J. Li, L. Xing, Z. Wang, W. Tu, X. Yang, Y. Lin, Y. Liao, M. Xu, and W. Li, *RSC Adv.*, **8**, 25794 (2018).
31. A. Nurpeissova, D.-I. Park, S.-S. Kim, and Y.-K. Sun, *J. Electrochem. Soc.*, **163**, A171 (2016).
32. X. Zuo, C. Fan, X. Xiao, J. Liu, and J. Nan, *J. Power Sources*, **219**, 94 (2012).
33. S. Wu, Y. Lin, L. Xing, G. Sun, H. Zhou, K. Xu, W. Fan, L. Yu, and W. Li, *ACS Appl. Mater. Interfaces*, **11**, 17940 (2019).
34. M.-S. Song, R.-H. Kim, S.-W. Baek, K.-S. Lee, K. Park, and A. Benayadr, *Journal of Materials Chemistry A*, **2**, 631 (2014).
35. M. Xu, L. Zhou, Y. Dong, Y. Chen, A. Garsuch, and B. L. Lucht, *J. Electrochem. Soc.*, **160**, A2005 (2013).
36. T. T. Hagos et al., *ACS Appl. Mater. Interfaces*, **11**, 9955 (2019).
37. G. Xu et al., *J. Power Sources*, **416**, 29 (2019).
38. S. K. Heiskanen, J. Kim, and B. L. Lucht, *Joule*, **3**, 2322 (2019).
39. C. Fu, J. Wang, J. Wang, L. Meng, W. Zhang, X. Li, and L. Li, *Journal of Materials Chemistry A*, **7**, 23149 (2019).